EFFECTS OF NOZZLE PERTURBATIONS ON TURBULENT MIXING IN IMPINGING JETS

Rong Ding, Johan Revstedt, Laszlo Fuchs
Department of Heat and Power Engineering,
Lund Institute of Technology
P.O. Box-118, Lund 22100, Sweden
Rong.Ding@vok.lth.se, Johan.Revstedt@vok.lth.se, Laszlo.Fuchs@vok.lth.se

ABSTRACT

The effect of the perturbations at the jet nozzle on the turbulent mixing in impinging jets is studied using simultaneous Particle Image Velocimetry (PIV) and Planar Laser-induced Fluorescence (PLIF) technique. The nozzle-to-wall distance H/D = 5.0 is investigated for turbulent jet flows at a Reynolds number of 6,000. The jet exit conditions are examined and typical flow structures in the jet are demonstrated. The unperturbed nozzle (N-0) is compared to nozzles with two (N-2) and three (N-3) needle shaped rods, respectively. The results show that the potential core is shorter in the N-2 and N-3 cases. This is caused by an earlier transition to turbulence and wider distribution of vorticity in the shear layer, which also leads to enhanced mixing indicated by the evolution of the dye tracer and the turbulent fluxes. The effect of the perturbation is also evident in other statistical properties, such as turbulent kinetic energy.

INTRODUCTION

Turbulent mixing behavior of a passive scalar in an impinging jet flow is very important in many industrial applications where chemical reactors and/or heat and mass transfer are essential. In an effort to enhance the mixing in such flows, a passive mixing-control strategy has been introduced in recent years by means of geometrical modifications of the jet nozzle, which can directly alter the flow development downstream relative to using a conventional circular nozzle. Recently, the strategy has been comprehensively reviewed by Gutmark and Grinstein (1999), including experimental, theoretical and numerical investigations. They reported that complex interactions between azimuthal and streamwise vortices in the noncircular free jets lead to increased entrainment characteristics and enhanced fine-scale mixing in the near jet field.

In the literature one may find several studies of passive control of mixing, mainly in free jets (Obot et al., 1979; Ashforth-Frost and Jambunathan, 1996). Using elliptic or rectangle nozzle indicate that the entrainment rates are significantly increased compared to conventional circular nozzle. Higher mixing rate has been observed in the former cases. Also, there is a reduction of the length of the potential core to three to four equivalent jet diameters compared to five diameters for the circular nozzle. Studies of jets issuing from nozzles with corners showed a substantial increase of the fine-scale turbulence at the corners and enhanced entrainment of mass. Another approach is to use axial vorticity generators, such as lobed nozzle (Hu et al. 2000), vortex generators (Mi and Nathan, 1999) or other shaping concepts (Reeder and Samimy, 1996). However, no studies have been reported about the effect of small, discrete rods fixed around the perimeter of the nozzle exit on the turbulent scalar mixing in impinging jets. This arrangement is proposed due to its simplicity and potential to be also used in active control environments.

In the experimental studies of turbulent mixing, it is of particular interest to measure the instantaneous velocity and concentration field simultaneously, since the mixing process can be described as the interaction between a velocity and concentration field. Whole-field simultaneous PIV/PLIF technique satisfies this requirement and has been successfully employed as a reliable, non-intrusive measurement technique in the jet mixing studies (Law and Wang, 2000; Borg et al., 2001). Using this technique, the turbulent fluxes $(-\overline{u_j' c'})$ can be measured directly. The turbulent fluxes can't be expressed analytically in terms of mean quantities. Hence, the essence of modelling of turbulent flows is to express the turbulent fluxes of different quantities. Historically, it has been difficult to directly assess different models due to the lack of experimental data. Now we can measure simultaneously both the local velocity (mostly in 2-D) and the concentration at the same time. Such data enables one to compute the turbulent fluxes of the concentration $(-\overline{u_j' c'})$. In particular, for the case of the impinging jet, the radial and axial turbulent fluxes $(-\overline{v'c'})$ and $(-\overline{u'c'})$ can be measured. This data can be directly used for assessing numerical models for turbulent heat- and mass-transfer.

Our objective of this study is to explore the effect of small perturbations near the nozzle on the mixing of spatially developing impinging jets. The experiments are to provide good quality data on the velocity and the concentration field as well as the turbulent fluxes for later comparison with Large Eddy Simulation (LES). In particular we focus on the deflection region. In present study, simultaneous PIV/PLIF has been used.

EXPERIMENTAL APPARATUS AND METHOD

The experiments are carried out in a closed-loop water system, as shown in Figure 1. The nozzle ($D = 20mm$) is fixed vertically in the middle of a test chamber ($20D \times 20D \times 22D$). The primary jet flow is supplied vertically by a pump and impinges perpendicularly onto a flat wall. The nozzle-to-wall distance H can be varied within a rather wide range ($0 \leq H/D \leq 12$). The flow rate of the jet is measured with a flow meter and controlled by a frequency converter. A pipe with a length of $30{\cdot}D$ and a cylindrical honeycomb chamber are installed upstream of the nozzle to ensure that the jet

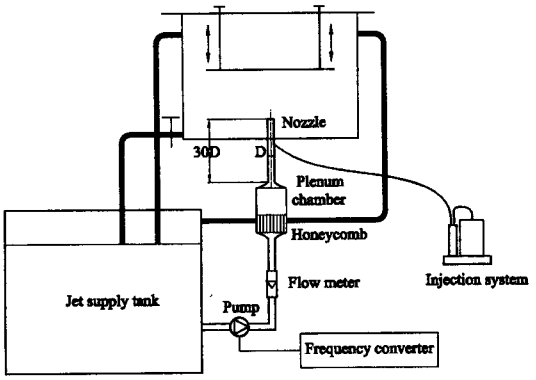

Figure 1: Flow facility.

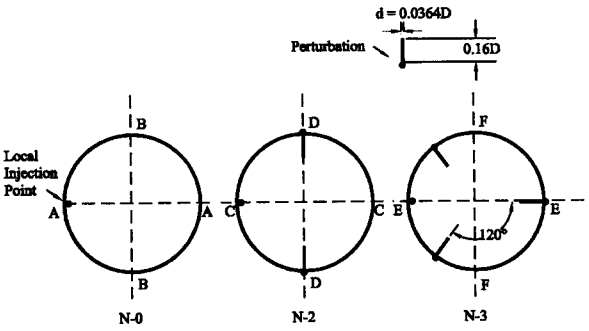

Figure 2: Front views of the three tested nozzles.

flow at the exit of the nozzle is fully developed. An overflow system is used to keep the water level in the test chamber at constant level during the experiments. The whole system has been found to be rather stable.

Three different nozzles, shown in Fig. 2, each with the same nominal diameter D, have been studied. The standard nozzle is circular and is designated N-0. The other two nozzles are designated N-2 and N-3 with the numeral indicating the number of small rods as shown in Fig. 2. These rods are needle shaped cylinders fixed at the exit circumference so that they perturb the flow. Each rod is approximately $0.0364{\cdot}D$ in diameter and length of $0.16{\cdot}D$ with an area blockage of 0.75% of nozzle cross section.

In the present study, the impingement distance is set to $5.0{\cdot}D$, while the jet Reynolds numbers (based on jet bulk velocity at the exit of the nozzle V_b, nozzle exit diameter D) is fixed at 6,000. The measurements have been carried out at the center plane of the jet (S_0) that contains the centerline of the jets for the three different nozzle configurations, respectively.

The closed-loop system is seeded with glass spheres with a mean diameter of 10 μm and a density of 1.10 g/cm^3 for PIV measurements. Adequate number of seeding particles are added to the water so that there are 10-15 particle images in one interrogation window but has no influence on the local fluorescent signal. A solution of Rhodamine B (SIGMA) at concentration C_0 is injected locally close to the pipe wall at the nozzle exit through a rigid tube ($d = 1.3mm$) by a piston injection system. The injection velocity (V_{inj}) is set to half of the mean jet bulk velocity. Analysis of the mean velocity profiles close to the inlet shows that this injection-

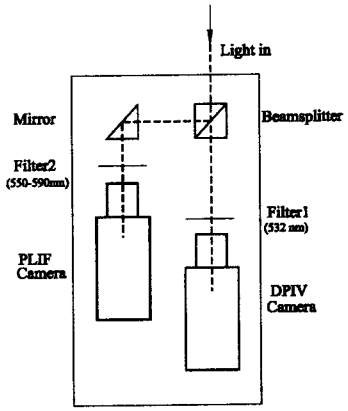

Figure 3: Detailed recording system for DPIV/PLIF measurement.

system does not disturb the jet velocity profiles.The solution of Rhodamine B and the injection velocity are kept constant for all three nozzles.

A double-pulsed Nd: YAG laser provides a green beam of light at a peak wavelength of 532 nm with a power of 25 mJ/pulse. The beam is passed through sheet forming optics to produce a thin laser sheet of measured thickness 1.5 mm, which illuminates the jet flow field for the combined PIV and PLIF measurements. The time delay between the two laser pulses is set to 2500 μs so that the particle-image displacement is about one-quarter of interrogation window, which is an optimum value (Adrian, 1991). Two high-resolution CCD cameras (Flow Master 3S, 1280×1024 pixels) equipped with different filters capture the images, as shown in Figure 3 in detail. Filter1 (Lavision BP 532/3) on the PIV camera passes the laser light at 532 nm and has a bandwidth of 3 nm. This filter blocks therefore effectively the yellow/orange fluorescent light emitted by the Rhodamine B dye while passing the green light scattered by the suspended particles. Filter2 (Melles Griot, OG530 and OG550) with cutoff around 560nm is placed on the PLIF camera to avoid any scattered light from the seeding particles used for PIV measurement. Meanwhile, the alignment between the two cameras is carefully adjusted, within 2 pixels, by means of a beam-splitter and mirror system. This arrangement allows us to simultaneously measure the (2-D) velocity field and the concentration field in the same plane. Double-exposure double frame mode and double-exposure single frame mode are chosen for PIV and PLIF measurements, respectively. The final spatial resolution for both PIV and PLIF images is about 114 $\mu m/pixel$ and the sampling rate is 4 Hz.

Cross-correlation algorithm is employed for processing the PIV images. Recent proposed enhancements, such as adaptive multi-pass correlation with deformed interrogation regions, local windows shift, are chosen to obtain the displacement (Westerweel et al., 2000). A cell size of 16 × 16 and a shift of 50% cell overlay are specified as the interrogation window for the PIV processing. Therefore, the final interrogation window size is 8 × 8 pixel. The corresponding concentration data are averaged over 8 × 8 subwindows during the PLIF image processing. Details concerning the PLIF technique and processing can be found in Ding et al. (2003) and Guillard et al. (1998).

The major source of errors are due to errors in estimating particle displacement, signal-to-noise ratio, accuracy of calibration curve for concentration measurement as well as

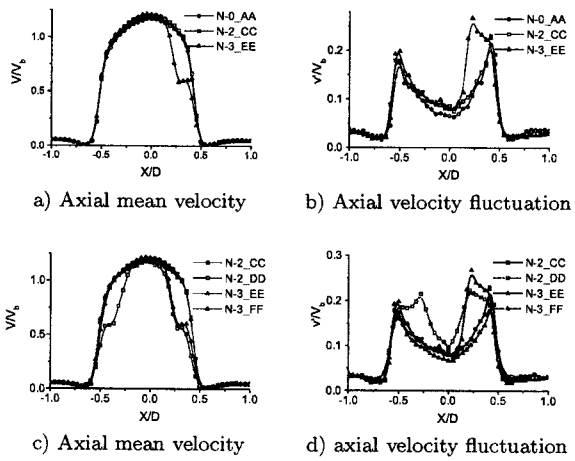

a) Axial mean velocity b) Axial velocity fluctuation

c) Axial mean velocity d) axial velocity fluctuation

Figure 4: Exit conditions of the jets without and with jet exit perturbations.

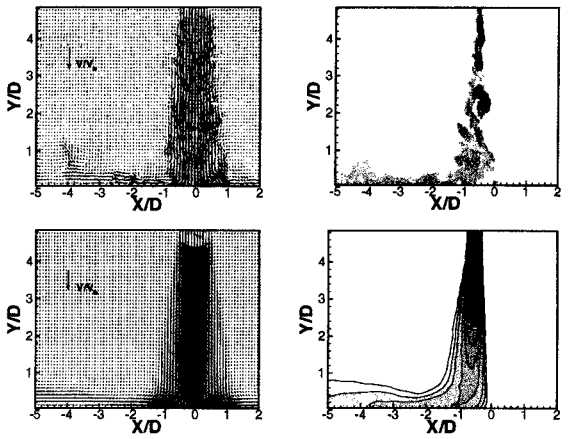

Figure 5: Simultaneous DPIV/PLIF measurement of a circular impinging jet in the center plane, (a) Instantaneous velocity field, b) Instantaneous concentration field, c) Mean velocity field, d) Mean concentration field

having a limited number of samples. In the present study, based on N = 650 images, the uncertainty in the mean velocity and concentration should be less than 5% and 7%, respectively. Hence, the uncertainties in the quantities presented herein and turbulent fluxes should be less than 8% and 12%, respectively.

RESULTS AND DISCUSSIONS

Jet Exit Condition and Sample Results

The nozzle outlet velocity conditions for the three cases at different planes (see Fig. 2) are shown in Figure 4 (a)-(d). These measurements have been done at $0.1{\cdot}D$ downstream of the nozzle exit. It is observed that at AA plane of N-0 jet (*N-0_AA*) and CC plane of N-2 jet (*N-2_CC*), the axial mean velocity and axial turbulence velocity profiles are within 5% difference. Relative turbulence peaks are close to the edge of the jet and reach approximately 18% of the jet bulk velocity (V_b). In the EE plane of N-3 jet (*N-3_EE*), the axial mean velocity is decreased up to $48\%{\cdot}V_b$ at $0.25{\cdot}D$ from the centerline of the jet and the axial turbulent velocity is increased at the corresponding position up to $22.5\%{\cdot}V_b$. The rod that is placed in the EE plane for the N-3 jet is the reason for this decreased axial mean velocity and increased turbulence velocity.

Flow asymmetry is observed in the velocity measurements in the plane perpendicular to CC plane of N-2 jet and EE plane of N-3 jet respectively, i.e, *N-2_DD*, *N-2_FF*. As shown in Figures 4 (c)-(d), the presence of the rods change the axial velocity, leading to flow asymmetry as well as introducing high turbulence intensity.

Figure 5 (a)-(b) shows a simultaneous PIV/PLIF measurement result for case N-0. A low turbulent region can be seen evidently in the flow field about $0 - 1.0{\cdot}D$ downstream from the nozzle exit, which is also indicated by Hu et al. (2001). At the end of this low turbulence region, spanwise Kelvin-Helmholtz vortices rings roll up. The flow undergoes transition to turbulence at the entrance of the deflection region ($Y/D = 1.1 - 1.4$). After impingement onto the wall, the flow deflects and develops into a wall jet. In the range $Y/D = 0 - 3.5$ from the wall, the distribution of concentration contours evidently show that the interface of the jet shear layer to be highly affected by the presence of a large range of scales, i.e., large-scale coherent structures and fine-scale turbulence. Figures 5 (c)-(d) shows the ensemble-average velocity and concentration results of a conventional circular jet flow. The mean values are normalized with the jet bulk velocity $V_b = 0.31m/s$ and the jet reference concentration $C_0 = 78.8\mu g/l$, which is the maximum concentration on the line $Y/D = 3.0$. The development of the jet and the spreading of the dye tracer in the shear layer can be observed clearly in these two concentration images. As expected, the shear layer width increases with downstream distance and the entrainment of low-concentration, low-momentum fluid from the ambient into the jet, resulting in a decrease of the concentration of dye tracer and velocity magnitudes.

Flow Characteristic

To characterize the flow properties of jets with different nozzles, the normalized mean velocity (V/V_b) and the root-mean-square turbulent fluctuation (v'/V_b) on the axis of the jets for the three nozzles are shown in Figure 6. For the unperturbed case (N-0 jet), V/V_b decreases slowly as the jet approaches the stagnation point. Within about $0.7{\cdot}D$ from the wall, the velocity decreases abruptly mainly due to the strong effect of the wall. The turbulent fluctuations experience an almost opposite process: they increase slowly and reach their maximum at about $0.3{\cdot}D$ from the wall followed by a sudden decrease.

For the perturbed cases (N-2 and N-3 jets), the mean velocity has the same trend as for the reference case (for each perturbed jet, the difference in velocity characteristics obtained from the two perpendicular planes are less than 2% and the results are not shown here.). However, significant difference is found near the wall, i.e. the velocity of perturbed cases decay more quickly than the N-0 jets. Furthermore, the turbulence fluctuations increase considerably for the two cases with inlet perturbations. The peak turbulence intensity increases by about 15% and is attained more proximally than that for the conventional circular case. Increased turbulent fluctuations enhance certainly the turbulent mixing.

To show the reliability of the results, the mean axial velocity of conventional jet (N-0 jet) is compared with the data

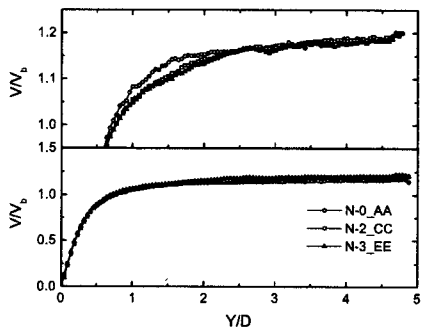

a) Axial mean velocity

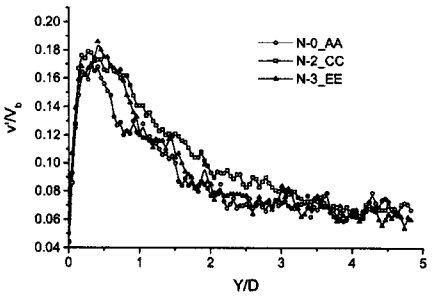

b) Axial velocity fluctuation

Figure 6: Evolution of axial mean velocity and turbulence fluctuation on the axis of the jets with different nozzles.

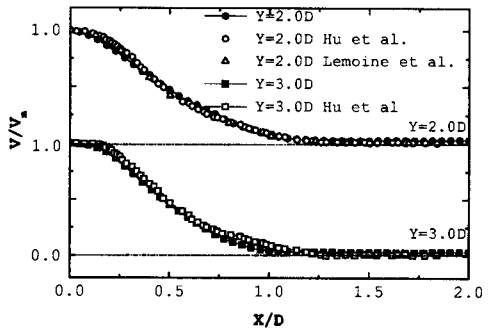

Figure 7: Axial mean velocity versus the radial direction.

from the literature (Lemoine et al., 1996 and Hu et al., 2001). Figure 7 shows the profiles of normalized mean axial velocity (V/V_m, where V_m is the maximum axial mean velocity on the jet axis) at $Y/D = 2.0$, 3.0 away from the impingement wall obtained in the current study and compared with the data obtained by PIV/PLIF measurement (Hu et al., 2001) and LDV/PLIF measurement (Lemoine et al., 1996) in the free jets. Since these data are all from the free jet region, they are comparable.

The modification of the jet flow field by the perturbations is also evident in other statistical properties, such as turbulent kinetic energy. Figure 8 shows the iso-contour of

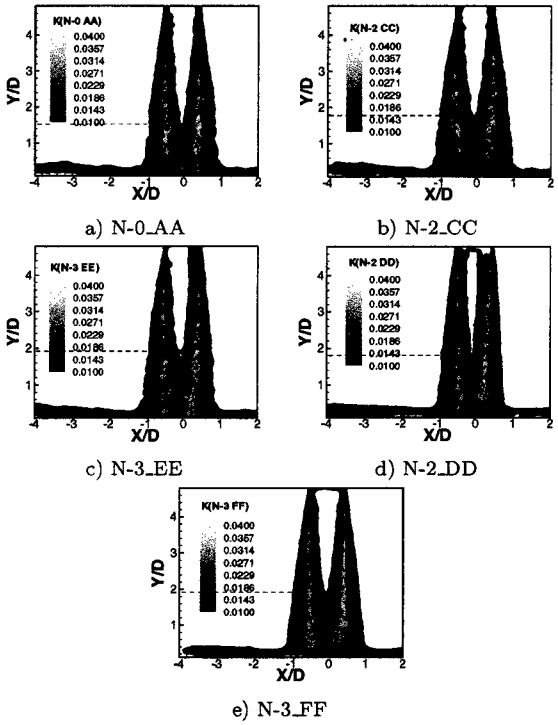

a) N-0_AA b) N-2_CC

c) N-3_EE d) N-2_DD

e) N-3_FF

Figure 8: Contours of turbulent kinetic energy.

turbulent kinetic energy k for three different nozzles.

From these plots, it can be observed that there exits a low turbulent intensity region (where $k \leq 0.01$) in the center of the turbulent jet flow. High levels of turbulent kinetic energy regions (where $k \geq 0.03$) exist in the shear layers between the jet flow and ambient flows. From comparison, the effect of the inlet perturbations on the iso-contour field of turbulent kinetic energy can be noted:

- For the unperturbed jet flow, the low turbulent intensity region of the jet extends downstream to $Y/D = 1.5$ from the wall, while this region of the perturbed jet flows is shorter than that of the unperturbed jets. Furthermore, the length of low turbulent intensity region is even shorter in the N-3 case than that in the N-2 case. Similar extent of low turbulent intensity region can be found in the two perpendicular plans of the jet flow (about $1.8{\cdot}D$ and $1.95{\cdot}D$ from the wall for N-2 and N-3 jets respectively).

- The expansion of the shear layer (the region where $k \geq 0.01$) for perturbed jet flow is wider than that in unperturbed jet flow in the near field of the jet.

- The intensive mixing regions (the regions where $k \geq 0.03$) for perturbed jet flow is found to appear more upstream and is wider than that in unperturbed cases.

Figure 9 shows the distribution of turbulent kinetic energy at three downstream locations $Y/D = 3.0$, 1.0 and 0.5. One can notice that the peaks of the turbulent intensity in the N-0 case are in the middle of the shear layer, which originates from the rim of the nozzle exit. The peaks of turbulent intensity are increasing downstream up to 0.35 on the line $Y/D = 1.0$ and then decreasing to 0.28 on the line $Y/D = 0.5$. With the development of the jet, the shear layer

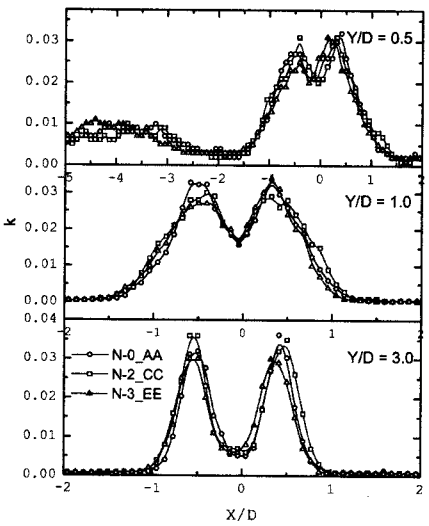

Figure 9: Axial evolution of turbulent kinetic energy for three nozzles.

entrains the ambient fluid and spreads in the spanwise direction. That is, it spreads from 1.0·D away from the jet axis on the line Y/D = 3.0 up to 1.5·D on the line Y/D = 1.0. Compared with N-0 case on the line Y/D = 3.0, 2.0, the N-2 case has more intense turbulence diffusion towards the outer edge of the jet, while the center of the N-3 case moves to one side as the flow evolves downstream. The increased turbulence intensity enhances the turbulent mixing. However, the peak of turbulence intensity for each line in the perturbed jets has more decays than the N-0 case. Furthermore, on the line Y/D = 0.5, big difference can be found in the wall jet region (from X/D = -2.0 to X/D = -5.0). The N-0 case shows the earliest appearance of the local maximum turbulence intensity along the impingement wall, while the N-3 case is the last one.

Mass Transport Characteristics

Figure 10 and 11 show the profiles of normalized concentration and concentration fluctuation at line Y/D = 1.0, 0.5 and 0.2 in the deflection region of the jet, respectively.

As shown in Figure 10, the effect of perturbations on the average concentration is clearly noticeable. At the entrance of the deflection region (i.e., Y/D = 1.0), the mixing is enhanced for the N-2 and the N-3 cases at the outer edge of the jet as compared to the N-0 case. Also, the N-0 case has faster spreading of the dye tracer towards the axis of the jet. In the deflection region (i.e. Y/D = 0.5, 0.2), faster spreading of the dye tracer can be observed for the N-2 and the N-3 cases. Most significant effect of the perturbations can be found on the line Y/D = 0.2. The secondary peak in the normalized mean concentration is found between X/D = -4.0 to X/D = -2.0. The values for each secondary peak is about 0.73, 0.60 and 0.49 for the N-0, N-2 and N-3 cases, respectively. The presence of these secondary concentration peaks is mainly due to the present primary vortices. For the N-0 case, primary vortices are larger compared to the N-2 and the N-3 cases, since the inlet perturbations accelerate the turbulence development.

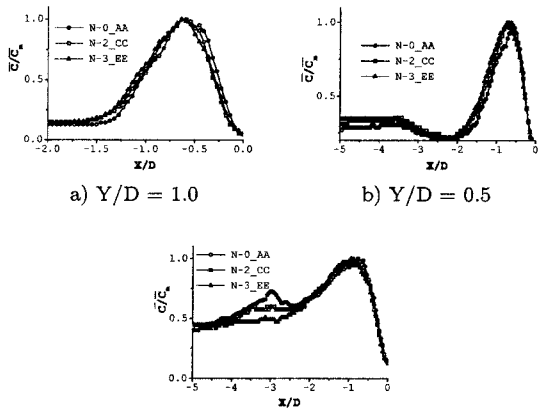

a) Y/D = 1.0 b) Y/D = 0.5

c) Y/D = 0.2

Figure 10: Normalized mean concentration at different axial sections without and with nozzle exit perturbations.

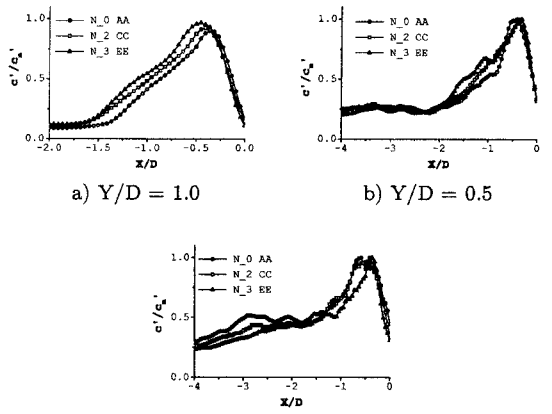

a) Y/D = 1.0 b) Y/D = 0.5

c) Y/D = 0.2

Figure 11: Normalized concentration fluctuation at different axial sections without and with nozzle exit perturbations.

From the concentration fluctuation at these three locations (shown in Fiure 11), it can be seen that the concentration fluctuation of the unperturbed jet is smaller than that of the perturbed jets at the edges of the shear layer. These observations show that the perturbed jets achieve a more-uniform mixing than the unperturbed jets.

Generally speaking, the effect of the perturbations on the concentration fluctuation is larger than that on the mean concentration value.

Turbulent fluxes of the tracer

The distribution of the turbulent fluxes of the scalar, i.e., $-\overline{v'c'}$, $-\overline{u'c'}$, across the jet for the three cases, is shown in Figure 12. The figure depicts the values normalized by the peaks of turbulent flux $-\overline{(v'c')}_{max}$, $-\overline{(u'c')}_{max}$ for each line, respectively.

As expected, the axial turbulent flux $-\overline{v'c'}$ for the N-0 case is symmetric around X/D = -0.5 near the exit (not shown here). Downstream, the profile presents an asymmetric shape with the shift of peaks to the jet axis. In fact, these maximum corresponds to the mixing layer of the jet, where

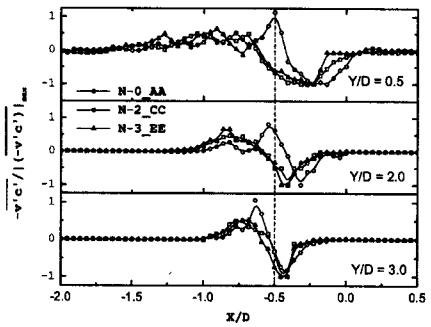

a) Axial turbulent scalar flux

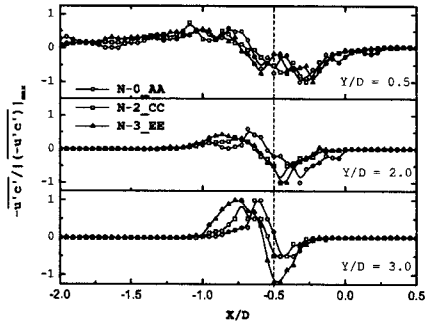

b) Radial turbulent scalar flux

Figure 12: Comparison of the normalized turbulent scalar flux across the three jets.

the Reynolds shear stresses and the concentration gradients reach a maximum. The radial turbulent flux $-\overline{u'c'}$ and axial turbulent flux $-\overline{v'c'}$ are found to be almost same shape from the present measurement results.

Compared with the unperturbed case, the value of turbulent fluxes for the perturbed cases are higher at the both edge of the mixing layer and have a shift from the unperturbed case. So the turbulent mixing process between the clear ambient water and the colored turbulent jet is enhanced by the presence of perturbations.

CONCLUSIONS

The effects of nozzle exit perturbations on turbulent mixing in impinging jets has been investigated using simultaneous PIV/PLIF. Flow and mixing characteristics at Reynolds number of 6,000 with H/D = 5.0 were measured in order to evaluate the effects of exit perturbations. Compared with the unperturbed jet (N-0 case), the length of low turbulent region in the jet core is 8.6% and 12.9% shorter in the N-2 and N-3 cases, respectively. Moreover, the mixing is enhanced in perturbed impinging jets indicated by the distribution of mean concentration and turbulent fluxes. The mixing enhancement is attributed to the fact that the nozzle exit rods produce a three-dimensional perturbations, leading to the early appearance of fine-scale turbulence in the near field and suppression of large-scale vortical structures in the wall-jet region.

Consequently, the nozzle exit rods can be used as an effective passive control technique for mixing enhancement for the practical applications.

ACKNOWLEDGMENT

This work was financially supported by the Swedish Research Council and the Swedish National Energy Administration (STEM).

REFERENCES

Adrian, R.J., 1991, "Particle-imaging technique for experimental fluid mechanics", *Annual Reviews in Fluid Mechanics*, Vol. 23, pp. 261-304.

Ashforth-Frost, S., and Jambunathan, K., 1996, "Effect of nozzle geometry and semi-confinement on the potential core of a turbulent axisymmetric free jet", *Int. Comm. Heat Mass Transfer*, Vol. 23, pp. 152-162.

Borg, A., Bolinder, J., and Fuchs, L., 2001, "Simultaneous velocity and concentration measurements in the near field of a turbulent low-pressure jet by digital particle image velocimetry-planar laser-induced fluorescence", *Exp. Fluids*, Vol. 31, pp. 140-152.

Ding, R., Guillard, F., and Fuchs, L., 2003, "A experimental study on the mixing in turbulent impinging jets", To be submitted for publication.

Guillard, F., Fritzon, R., Revstedt, J., Trägårdh, C., Aldén, M. and Fuchs, L., 1998, "Mixing in a confined turbulent impinging jet using planar laser-induced fluorescence", *Exp. Fluids*, Vol. 25, pp. 143-150.

Gutmark, E. J., and Grinstein, F. F., 1999, "Flow control with noncircular jets", *Annu. Rev. Fluid Mech.*, Vol. 31, pp. 239-72.

Hu, H., Kobayashi, T., Saga, T., Segawa, S., and Taniguchi, N., 2000, "Particle image velocimetry and planar laser-induced fluorescence measurements on lobed jet mixing flows", *Exp. Fluids.*, S: pp. S141-S157.

Hu, H., Sega, T., Kobayashi, T., and Taniguchi, N., 2001, "Simultaneous velocity and concentration measurements of a turbulent jet mixing flow", *Pro. of Int. Symp. on Visualization and Image in Transport Phenomena.*

Law, A. W. K., and Wang, H. W., 2000, "Measurement of mixing processes with combined digital particle image velocimetry and planar laser induced fluorescence", *Exp. Therm. Fluid Sci.*, Vol. 22, pp. 213-229.

Lemoine, F., Wolff, M., and Lebouche, M., 1996, "Simultaneous concentration and velocity measurements using combined laser-induced fluorescence and laser Doppler velocimetry: Application to turbulent transport", *Exp. Fluids*, Vol. 20, pp. 341-327.

Mi, J. and Nathan, G. J., 1999, "Effect of samll vortex-generators on scalar mixing in the developing region of a turbulent jet", *Int. Heat and Mass Transfer*, Vol. 42, pp. 3919-3926.

Obot, N. T., Majumdar, A. S., and Douglas, W. J. M., 1979, "The effect of nozzle geometry on impingement heat transfer under a round jet", *ASME paper NO. 79-WA/HT-53.*

Reeder, M. F., and Samimy, M., 1996, "The evolution of a jet with vortex-generating tabs: real-time visualization and quantitative measurements", *J. Fluid Mechanics*, Vol. 311, pp. 73-118.

Westerweel, J., Dabiri, D., and Gharib, M., 2000, "The effect of a discrete window offset on the accuracy of cross-correlation analysis of digital PIV recordings", *Exp. Fluids*, Vol. 23, pp. 20-28.